Title
Probing the Ion Transport Properties of Ultrashort Carbon Nanotubes Integrated with Supported Lipid Bilayers via Electrochemical Analysis.

Journal
Journal of Physical Chemistry B (Soft Condensed Matter and Biophysical Chemistry), 127(28)

Authors
Park, Yunjeong
Hong, Minsung
Kim, Teayeop
et al.

Publication Date
2023-07-20

DOI
10.1021/acs.jpcb.3c02917

Peer reviewed

THE JOURNAL OF PHYSICAL CHEMISTRY B
A JOURNAL OF THE AMERICAN CHEMICAL SOCIETY

pubs.acs.org/JPCB

Article

Probing the Ion Transport Properties of Ultrashort Carbon Nanotubes Integrated with Supported Lipid Bilayers via Electrochemical Analysis

Yunjeong Park,[¶] Minsung Hong,[¶] Teayeop Kim, Hyeonseo Na, Sunho Park, Yeon Ju Kim, Jangho Kim, Yun-Hoon Choung, and Kyunghoon Kim*

Cite This: *J. Phys. Chem. B* 2023, 127, 6316−6324

Read Online

ACCESS | Metrics & More | Article Recommendations | Supporting Information

ABSTRACT: Supported lipid bilayers (SLBs) are commonly used to investigate interactions between cell membranes and their environment. These model platforms can be formed on electrode surfaces and analyzed using electrochemical methods for bioapplications. Carbon nanotube porins (CNTPs) integrated with SLBs have emerged as promising artificial ion channel platforms. In this study, we present the integration and ion transport characterization of CNTPs in *in vivo* environments. We combine experimental and simulation data obtained from electrochemical analysis to analyze the membrane resistance of the equivalent circuits. Our results show that carrying CNTPs on a gold electrode results in high conductance for monovalent cations (K^+ and Na^+) and low conductance for divalent cations (Ca^{2+}).

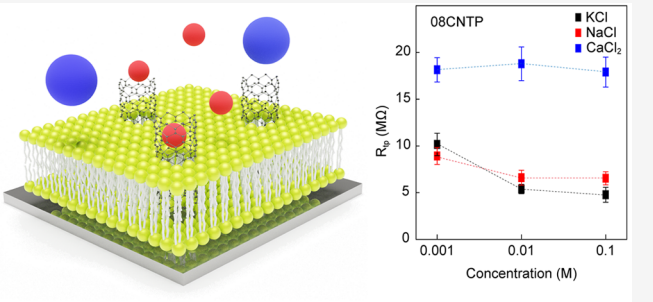

INTRODUCTION

The lipid bilayer is a fundamental component of biological membranes and has been extensively studied in terms of ion flux, biomolecule binding, and interactions between cells and their environment.[1−3] Supported lipid bilayers (SLBs) have recently emerged as promising sensor platforms, composed of a biolayer of phospholipids on a solid substrate. They provide a model for cell interfaces and facilitate integration with proteins, peptides, and transmembrane channels.[4−6] These channels incorporated into SLBs can be designed as ion sensors that exhibit selective ion transport and blocking, thus improving their functionality and creating a biomimetic environment similar to that of cell membranes.[7,8] SLBs with channel platforms have potential applications in bioanalytical and diagnostic fields, including drug screening and ion sensing.[9,10]

Advances in technology have led to an increased demand for functional transmembrane channels, and carbon nanotubes (CNTs) have been extensively studied for their ability to act as transmembrane proteins, such as α-hemolysin, aquaporins-1, and gramicidin.[11−16] CNT porins (CNTPs), which are CNT fragments with a length of ∼10 nm, have been obtained using lipid surfactants.[16] Previous studies have shown that CNTPs can be perpendicularly embedded into lipid vesicles, forming transmembrane channels that are similar to biological ion channels. The inert smooth surface of CNTPs enables the creation of favorable conditions for ion transport, and they can effectively prevent fouling components of biological mixtures from reaching sensor surfaces.[17]

In previous studies, the majority of CNTP analyses have primarily focused on patch-clamp measurements, emphasizing single-channel ion transport properties.[12,13,16] Despite the numerous studies on CNTPs, there is a limited understanding of the transmembrane properties of large-scale CNTP and SLB hybrid structures on solid substrates for sensor platforms. Several studies have demonstrated the successful insertion of CNTPs into lipid bilayers, investigating their transport properties and potential applications. For instance, Tunuguntla et al.[13] reported enhanced water permeability and tunable ion selectivity in sub-nanometer CNTPs. Additionally, Choi et al.[18] provided insights into the CNTP formation in lipid membranes, showing that CNTP can be inserted horizontally into the lipid bilayer.

Building upon these findings, this study aims to provide a proof of concept for the integration of CNTPs into a lipid bilayer on a gold electrode for analyzing ionic permeability at the microscale. To achieve this, we utilized electrical impedance spectroscopy (EIS) analysis, which applies an alternating current and can be used as a macroscale characterization method for transport studies in membranes.

Received: May 3, 2023
Revised: June 12, 2023
Published: July 11, 2023

https://doi.org/10.1021/acs.jpcb.3c02917
J. Phys. Chem. B 2023, 127, 6316−6324

EIS analysis is expected to facilitate the use of CNTP-SLB hybrid structures for biological applications at a cellular scale. We investigated ion transport through CNTPs with two different diameters (0.8 and 1.8 nm) using K^+, Na^+, and Ca^{2+} ions, which have different hydration radii. We demonstrated the formation of SLBs and the incorporation of CNTPs using a quartz crystal microbalance with dissipation (QCM-D), fluorescence imaging, and cyclic voltammetry (CV) analysis. EIS analysis was performed to characterize the ion transport through the CNTPs. The incorporation of CNTPs into the SLB led to a higher ion conductivity, which can be adjusted to tune the SLBs' insulating properties.

Our findings suggest that CNTP-SLB hybrid structures can be used as an effective platform for ion sensing and transport studies at the macroscale. The use of EIS analysis provides a promising method for the macroscale characterization of ion transport in membrane systems. This study expands our understanding of CNTP-SLB hybrid structures and paves the way for further exploration of their potential application in biological systems.

MATERIALS AND METHODS

Materials. The CNTs with diameters of 0.8 nm (08CNTs) and 1.8 nm (18CNTs), along with potassium chloride, sodium chloride, and calcium chloride, were obtained from Sigma-Aldrich. Additionally, 1,2-dioleoyl-*sn*-glycero-3-phosphocholine (DOPC) with a concentration of 25 mg mL^{-1} in chloroform was purchased from Avanti Polar Lipids.

Synthesis of CNTPs. Acid-treated CNTs were prepared according to a previously reported method.[19] The chemical oxidation process utilized a sulfuric acid/nitric acid mixture (H_2SO_4/HNO_3) to obtain carboxylic acid-functionalized CNTs (CNT-COOH). Briefly, CNTs (20mg) underwent oxidation in a 20 mL vial containing 2 mL of H_2SO_4/HNO_3 (3:1, v/v) for 24 h at room temperature with magnetic stirring (100 rpm). After washing with deionized (DI) water, CNT-COOH was collected by vacuum filtration on a 200 nm poly(tetrafluoroethylene) (PTFE) filter paper, which was purified by filtering 3 times with DI water (20 mL).

To prepare the CNTPs, 0.8 mL of DOPC suspension in chloroform was added to a 20 mL glass vial, and the N_2 gas gently evaporated the solvent. The vial was maintained under vacuum overnight to facilitate evaporation. Afterward, the dried lipid film vial received either 1 mg of pristine 08CNTs or acid-treated 18CNTs, referred to as CNT-COOH, following previously reported methods.[12,19] The addition of 20 mL of DI water followed, and the lipid/CNT suspensions were bath-sonicated for 1 h to distribute the CNTs in the lipid solution. Probe sonication with a 3 mm tapered microtip at 125 W for 16 h (VC505, Sonics) cut the CNTs into short fragments. The sonication ran in 3 s pulses with a 1 s pause between pulses, conducted in a cool environment to prevent vial overheating. After probe sonication, metal particles and large CNT aggregations were filtered using a 200 nm polycarbonate filter.

The sonication-processed solution was centrifuged at 6000*g* for 1 h at 24 °C to separate shortened CNTPs from uncut CNTs, causing the long CNTs to sink. By using a glass pipette, 8 mL of the upper supernatant containing short CNTs was collected and designated as 08CNTPs and 18CNTPs, based on their respective diameters.

CNTP Characterization. The transmission electron microscopy (TEM) images verified the diameter of bare CNTs (08CNTs and 18CNTs) (see Figure S1). The size of the CNTPs was characterized using dynamic light scattering (DLS) (Zetasizer S90, Malvern Inst., Germany), and each size was measured more than 10 times. Additionally, the CNTPs were characterized using Raman spectroscopy (XperRam 200VN, Nanobase) with a 512 nm wavelength laser and ultraviolet−visible spectrophotometry (UV−vis; i9, Hanon) to confirm the formation of CNT structures with few defects, compared to the bare CNTs.

Liposome and CNTP-Liposome Preparation. 1 mg of dried DOPC was prepared using N_2 gas and was evaporated overnight. Liposomes were prepared by adding 1 mL of DI water to the dried film to obtain a final lipid concentration of 1 mg mL^{-1}. This solution was hydrated at room temperature for 30 min and then bath-sonicated for 10 min. 10 cycles of freeze−thaw processes were conducted with liquid nitrogen and 60 °C DI water to form unilamellar vesicles. The unilamellar liposomes were extruded 21 times using a mini-extruder with a 50 nm pore-sized polycarbonate membrane (Avanti Polar Lipids).

During the rehydration process, prior to the freeze−thaw cycles, the CNTP solution was introduced to facilitate the incorporation of CNTPs into the liposomes. To verify the successful integration of CNTPs into the lipid bilayer, high-resolution cryo-transmission electron microscopy (Cryo-TEM) was employed. The representative Cryo-TEM image (see Figure S2) provides a visual confirmation of CNTPs in a transmembrane orientation within the lipid vesicles, supporting the integrity of our methodology and subsequent results.

QCM-D Measurements. The QCM-D technique (Q-sense E4, Q-sense AB, Sweden) was used to characterize the formation of SLBs and the integration of CNTPs. Prior to measurement, the quartz crystal sensors in the flow cell were cleaned using O_2 plasma (60 W, 3 min), and the temperature was set at 24 °C to minimize thermal effects. A peristaltic pump was used to regulate the flow rate to 50−100 μL min^{-1}, and the measurements were allowed sufficient time to ensure that the frequency and dissipation changes were less than 1 Hz and 0.2×10^{-6} in 10 min, respectively. Vesicle adsorption was monitored by changing the resonance frequency (Δf) and energy dissipation (ΔD) using several overtones, and all QCM-D data presented in this study were measured at the 5th overtone.

Electrochemical Analysis. The electrochemical tests were performed using a three-electrode system connected to a potentiostat (VSP 300, Bio-Logic SAS, Seyssinet-Pariset, France) and a commercially purchased screen-printed carbon electrode (SPCE; DS 200AT, Metrohm, Herisau, Switzerland). The working electrode (WE) and counter electrode (CE) were printed using gold ink, and the reference electrode (RE) was printed using silver/silver chloride ink. CV tests were conducted in a voltage range of 0−0.5 $V_{Ag/AgCl}$ with a scan rate of 10 mV s^{-1} to determine the charge-transfer resistance, while CV tests were conducted in a 10 mM $[Fe(CN)_6]^{3-/4-}$ redox agent. EIS tests were performed in the frequency range of 10 kHz to 0.1 Hz with an amplitude of 10 mV, and the solutions for the EIS tests were prepared with ion concentrations of 0.001, 0.01, and 0.1 M, respectively, for K^+, Na^+, and Ca^{2+}. The impedance plots were then analyzed using a suitable equivalent circuit and fitting process with the ZSimpWin software (ZSimpWin 3.20, EChem Software, Ann Arbor, MI).

https://doi.org/10.1021/acs.jpcb.3c02917
J. Phys. Chem. B 2023, 127, 6316−6324

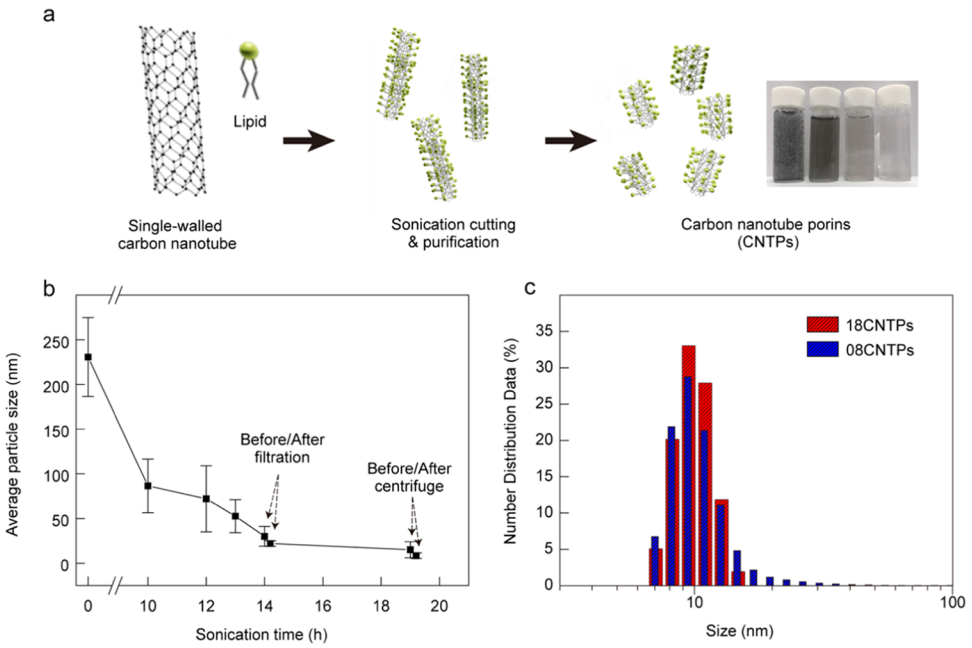

Figure 1. Fabrication of CNTPs. (a) Schematic of the CNTP synthesis procedure: cutting and purification. Inset: a photograph of CNT dispersion (from left to right, last vial: DI water). (b) Plot of the average particle size measured using DLS as a function of sonication time and the purification process. (c) Histogram of the hydrodynamic lengths of 08CNTPs and 18CNTPs.

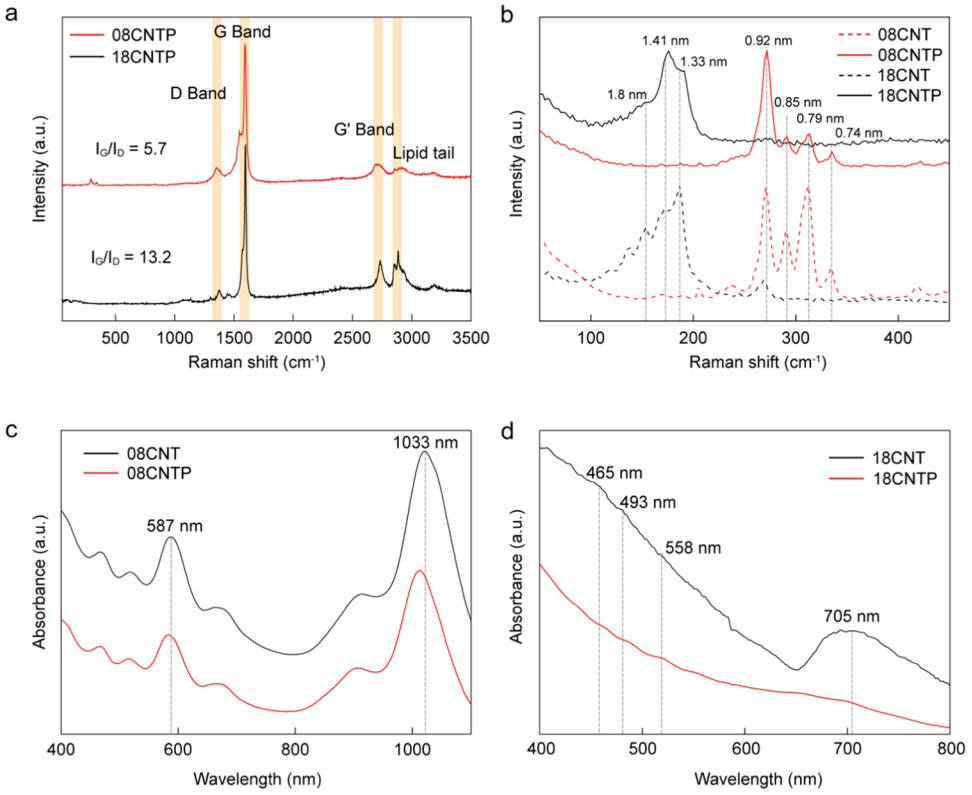

Figure 2. Characterization of CNTPs. (a) Raman spectra of 08CNTPs (red) and 18CNTPs (black). (b) Enlargement of the RBM region of the spectra provided in panel (a); uncut CNTs (dashed lines) and CNTPs (solid lines). (c, d) UV−vis-NIR absorption spectra of 08CNTs, 18CNTs, 08CNTPs, and 18CNTPs. Dashed lines indicate the location of major spectral features.

RESULTS AND DISCUSSION

Synthesis and Characterization of CNTPs. In order to make CNTs biocompatible, it is necessary to separate bundled CNT aggregates and cut them into individual fragments of 10−15 nm in length. To fabricate CNTPs, bundled CNTs were treated with acid and purified with DI water, resulting in the breakdown of the CNTs into smaller fragments.[12,19] The lipid film of DOPC and acid-treated CNTs were mixed together in a CNT suspension using bath sonication. The suspension was then cut using probe ultrasonication, which

https://doi.org/10.1021/acs.jpcb.3c02917
J. Phys. Chem. B 2023, 127, 6316−6324

caused microbubbling and cavitation at the CNT surface, resulting in the cutting of CNTs to yield fragments of smaller lengths. After 14 h of ultrasonication, the CNTs were filtered using a 200 nm polycarbonate filter and purified via ultracentrifugation so that the longer CNTs sank to the bottom of the conical tube. The top of the suspension solution was then extracted (see Figure 1a). After treatment, the aliquots exhibited a light gray color compared to the DI water and preprocessed samples (see Figure 1a, inset). The 08CNTs and 18CNTs underwent identical processes, and the processed CNTs were denoted 08CNTPs and 18CNTPs, respectively.

The lengths of the CNTs were analyzed using dynamic light scattering (DLS) (see Figure 1b,c). DLS with hydrodynamic radius measurements revealed the average sizes of the CNTPs for the two samples obtained after the filtration and centrifugation processes. The CNTP samples were ∼5 to 25 nm in length, and Figure 1b,c shows the CNT size distribution.

Raman spectra showed that the main characteristic peaks of CNTs, namely, the G, G′, and D bands, were observed at 1590, 2600, and 1310 cm^{-1}, respectively, for the two CNTP samples, as shown in Figures 2a,b and S3. The spectra confirmed that the CNTP structure was composed of CNT pores surrounded by DOPC lipids. The *G* and *G*′ bands represent the pristine graphitic structure of CNT, while the D band is associated with structural disorder introduced by defects and functional groups present on the CNT surface.[21] The I_G/I_D ratios of 5.7 and 13.2 for 08CNTPs and 18CNTPs, respectively, indicated that the good-quality graphitic structure was retained in the procedure for CNTP synthesis.[11] Additionally, a low-intensity broad peak at 2800 cm^{-1} corresponding to lipid tail peaks of C−H bond stretching was observed.[20] This observation suggests that lipids indeed surround the CNTs, forming the CNTPs.[20,21]

The characteristic radial breathing modes (RBMs) of the CNTs were also observed.[21] Comparing the RBMs at 50−500 cm^{-1} in the spectra of the raw CNT (08CNTs and 18CNTs) and CNTP (08CNTPs and 18CNTPs) samples revealed that the CNT diameters remained unchanged after probe ultrasonication and additional purification processes, as shown in Figure 2b. Specifically, in the 08CNT sample, the peaks observed at 270.6, 290.3, 312.1, and 336.1 cm^{-1} corresponded to diameters of 0.92, 0.85, 0.79, and 0.74 nm, respectively. For the 18CNT sample, the peaks observed at 138, 171.3, and 186.8 cm^{-1} corresponded to the diameters of 1.8, 1.41, and 1.33 nm, respectively, confirming their diameter distribution. Furthermore, the RBM region that revealed the diameter distribution in the uncut (08CNTs and 18CNTs) and porin (08CNTPs and 18CNTPs) samples displayed peaks at similar positions but with different relative intensities. This difference indicates that smaller-diameter CNTs are preferentially removed during the fabrication process, resulting in a higher proportion of larger-diameter CNTs remaining in the sample. Despite these differences, the 08CNTPs and 18CNTPs were successfully fabricated and are suitable for use in this study.

The UV−vis spectra presented in Figure 2c indicate that the E_{22} (587 nm) and E_{11} (1033 nm) optical transitions correspond to the electronic state densities of the 08CNT and 08CNTP samples after the cutting process.[22] Previous studies have suggested that, as the nanotube length decreases to a few nanometers, the exciton lifetime also decreases, leading to spectral peak broadening.[23,24] Additionally, a decrease in CNT length results in increased quantum confinement along the CNT axis, causing a blue shift in the absorbance peaks.[25]

Contrasting the 08CNTs and 08CNTPs, a noticeable broadening of peaks is observed for the 18CNTP compared to the 18CNT spectra (Figure 2d). The broadening of the 18CNTP UV−vis-NIR spectrum with faint peaks at 465, 493, 558, and 705 nm suggests the presence of 18CNTPs, albeit less distinct. This broadening, compared to the 08CNTP spectrum, might be attributed to differences in the confinement effect experienced by wider tubes. Wider tubes exhibit a less pronounced confinement effect, which can lead to a higher density of electronic states and a more complex energy landscape, resulting in a broader and more featureless spectrum. These results confirm that sonication caused significant changes in the CNT length while maintaining the intrinsic structure.

Optimization of Lipid Bilayer Formation on Au Electrodes via QCM-D and CNTP Insertion. The vesicle fusion method is a widely used technique for creating supported lipid bilayers (SLBs) on solid substrates like SiO_2, TiO_2, and Au, making them ideal for various bioanalytical models and sensing platforms.[26−28] However, oxide-based surfaces have limitations in sensing applications, such as low signal transduction between the sensor and biomolecules, due to electrical insulation. An alternative approach is to form SLBs on a gold surface, which allows for electrical and optical analyses, including electrochemistry and surface plasmon resonance.[29,30] The conductive properties of Au, combined with the insulating properties of SLBs, are also advantageous for the fabrication of biomimetic sensors based on biomolecules and ion conductance measurements.[31] Therefore, SLBs on a gold surface are highly suitable for various sensing applications.

To form high-quality SLBs on Au electrodes with minimal defects, we utilized QCM-D, a powerful tool for real-time monitoring of interactions between adsorbed layers and the surface. This technique detects mass-related changes as the frequency and dissipation of the gold-coated quartz sensor chip change.[31,33] For the efficient formation of planar SLBs on Au electrodes, we used the amphipathic-helix (AH) peptide of the hepatitis C virus NS5A protein with an N-terminus.[34] This peptide has been shown to destabilize intact lipid vesicles on gold surfaces, enabling the rupture process required for forming a planar lipid bilayer.[31,34]

The resonance frequency and dissipation shifts observed in QCM-D were in accordance with trends reported in previous publications on SLBs on Au quartz crystal sensors.[33−36] The process can be described in the following steps:

(i) Rinsing the Au-coated quartz sensor chip with a PBS buffer established a steady Δf and dissipation baseline at ∼0 Hz and 10×10^{-6}, respectively.

(ii) Introducing 50 nm unilamellar vesicles at a concentration of 0.1−0.2 mg mL^{-1} resulted in a significant decrease in frequency and an increase in dissipation due to the adsorption of intact vesicles onto the sensor chip, leading to the formation of a vesicle layer (increase of mass: see Figure S4a).

(iii) Subsequent rinsing with PBS eliminated the suspended vesicles and reduced the interaction between the remaining vesicles on the sensor surface.

(iv) The addition of the AH peptide at a concentration of 50 ng mL^{-1} induced a notable decrease in Δf and a corresponding increase in dissipation within a short period, suggesting an increase in mass. However, after 10

https://doi.org/10.1021/acs.jpcb.3c02917
J. Phys. Chem. B 2023, 127, 6316−6324

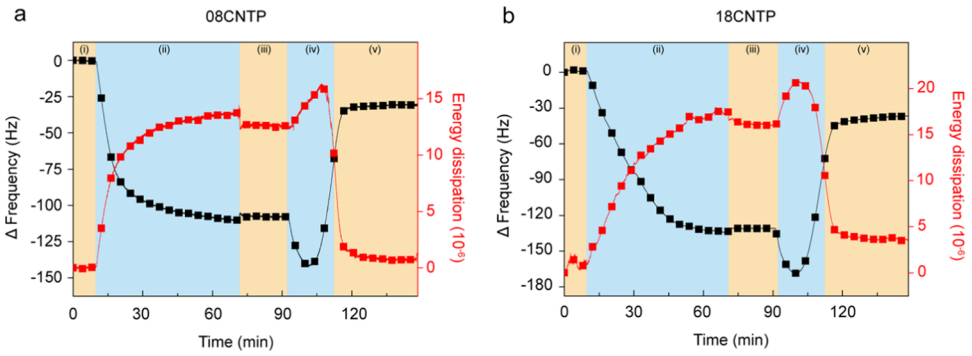

Figure 3. Optimization of lipid bilayer formation on the Au electrode and CNTP incorporation. Left axis: frequency analysis; right axis: dissipation analysis. (a) Insertion of the vesicle incorporated with 08CNTPs following the lipid bilayer formation process. (b) Insertion of the vesicle incorporated with 18CNTPs following the lipid bilayer formation process.

min, a substantial increase in Δf and a decrease in dissipation were observed, indicating a decrease in mass.

(v) Upon completion of the washing process, and once the sensor had reached a stable state, a significant reduction in both frequency and dissipation was observed in the convergence values. This change resulted from the formation of SLBs on the Au-coated quartz sensor, as the AH peptide triggered vesicle ruptures and the release of trapped water, resulting in a decrease in mass and dissipation. The vesicles then transitioned to a rigid lipid bilayer film, with the frequency and dissipation values reaching characteristic stable values (see Figure S4b).

As depicted in Figure S4, the vesicles are observed to be irreversibly adsorbed onto the substrate while remaining unruptured (see Figure S4a). The introduction of the AH peptide to the system destabilizes the vesicle structures, likely through electrostatic interactions that serve as the driving force for vesicle rupture.[34] Upon expanding and rupturing, the vesicle forms an SLB with final Δf and dissipation response values of 25 ± 0.3 Hz and less than 0.1 × 10^{-6}, respectively (see Figure S4b). The AH peptide does not contribute any mass to the supported bilayer, resulting in a complete SLB.

In order to evaluate the formation of a functional lipid bilayer, we introduced CNTPs, which serve as transmembrane channels in the SLBs. To accomplish this on the Au electrode, we prepared two types of CNTPs (08CNTP and 18CNTPs) by incorporating them into unilamellar vesicles (see Figure S2). The CNTPs can be successfully inserted into lipid vesicles, such that the CNTP-incorporated vesicle remains intact on the electrode, exhibiting high frequency and energy dissipation values similar to those of intact bare vesicles (Figure 3a,b (i)−(iii)). Following the addition of the AH peptide to induce vesicle rupture and the subsequent washing process, the frequency and dissipation values demonstrate the stable incorporation of these artificial channels (Figure 3a,b (iv),(v)). Furthermore, the absence of an abrupt change in dissipation suggests that the rigidity of the layer has not significantly altered, indicating the successful incorporation of CNTPs into the bilayer (Figure 3a,b (iv),(v)).

As shown in Figure 3a, the vesicle containing 08CNTPs exhibits final frequency and dissipation values of 30 ± 1 Hz and <3.6 × 10^{-6}, respectively. In Figure 3b, the vesicle incorporated with the 18CNTP has a final frequency and dissipation values of 40 ± 1.2 Hz and <0.5 × 10^{-6}, respectively. Using the Voinova viscoelastic model from a previous study,[37] we estimate that the CNTPs can achieve surface coverage of ~3.54 and 5.3% on the sensor surface. It is important to note that this estimation may represent an upper limit since the calculation assumes a flat surface.

The roughness of the Au surface significantly impacts the formation and stability of SLBs. A smoother Au surface typically provides more favorable conditions for vesicle adsorption and subsequent rupture, resulting in the formation of uniform and stable SLBs. On the other hand, a rougher Au surface may lead to incomplete bilayer formation or increase defect density due to irregularities and varying coverage. In our study, we prepared the Au surface to optimize the balance between surface roughness and SLB formation. This optimization is crucial for the formation of defect-free SLBs on the Au surface, particularly when incorporating CNTPs as transmembrane channels. Our experiments employed QCM-D measurements and analysis of frequency and dissipation values to confirm the successful formation of SLB from vesicles containing CNTPs.

Characterization of Lipid Bilayer Formation on the Au Electrode Using Fluorescence Recovery after Photobleaching (FRAP). To further verify the formation of SLB on the Au electrode, we employed fluorescence recovery after photobleaching (FRAP) as an optical method to determine the fluidity of the lipid molecules on the electrodes. In this experiment, we incorporated Rho-PE (1,2-dioleoyl-*sn*-glycero-3-phosphoethanolamine-*N*-(lissamine rhodamine B sulfonyl) (ammonium salt)), a fluorophore-labeled lipid, into the DOPC lipid (0.1 wt %) to facilitate the tracking of lipid molecule movement. During the FRAP process, the fluorophore-labeled lipid molecules within a specific region of interest (ROI) on the electrode surface were irreversibly photobleached using a 512 nm laser. A circular region with a 20 μm diameter was selected as the ROI, and the laser power was adjusted to ensure efficient photobleaching while minimizing the potential for photodamage to the lipid bilayer. Subsequently, we monitored the recovery of fluorescence within the ROI, which would indicate the lateral diffusion of unbleached Rho-PE-labeled lipids into the photobleached area. Within 10 min, a significant recovery of fluorescence was observed (see Figure S5), signifying the mobility and diffusion of lipids on the Au electrode surface. The diffusion coefficient, calculated from the FRAP data, was found to be D = 4.86 cm^2 s^{-1}, which is in line with previous studies on similar systems.[7,9] This result not only confirms the presence of a fluid lipid bilayer on the Au electrode but also supports the vesicle rupture observed in the QCM-D measurements.

https://doi.org/10.1021/acs.jpcb.3c02917
J. Phys. Chem. B 2023, 127, 6316−6324

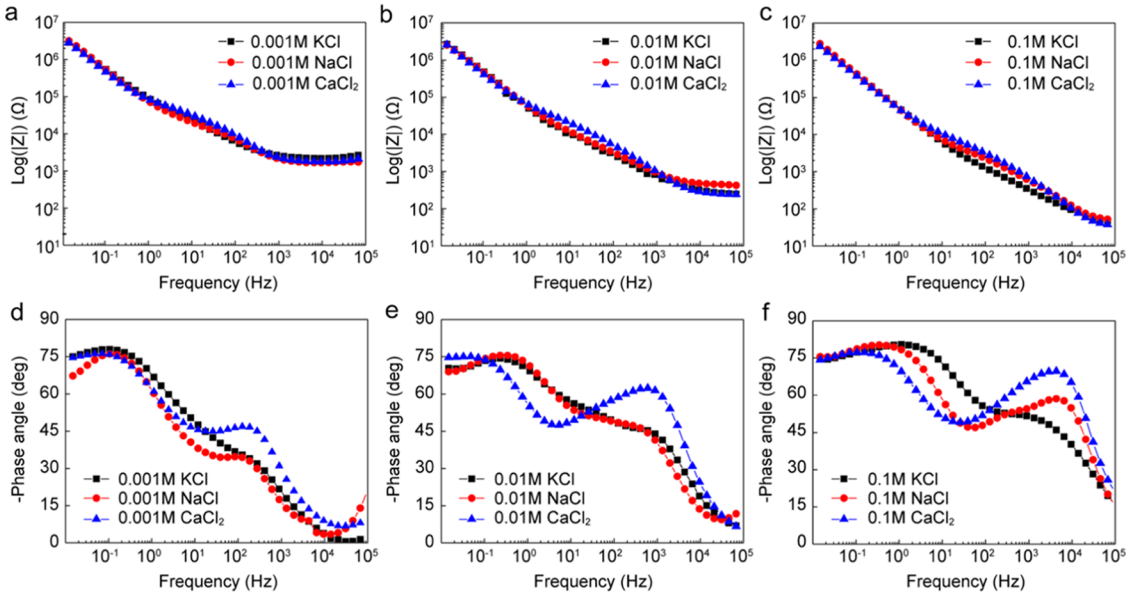

Figure 4. EIS results for 08CNTPs with a lipid bilayer according to cation and concentration: impedance of (a) 0.001 M, (b) 0.01 M, and (c) 0.1 M solution and phase angle of (d) 0.001 M, (e) 0.01 M, and (f) 0.1 M solution.

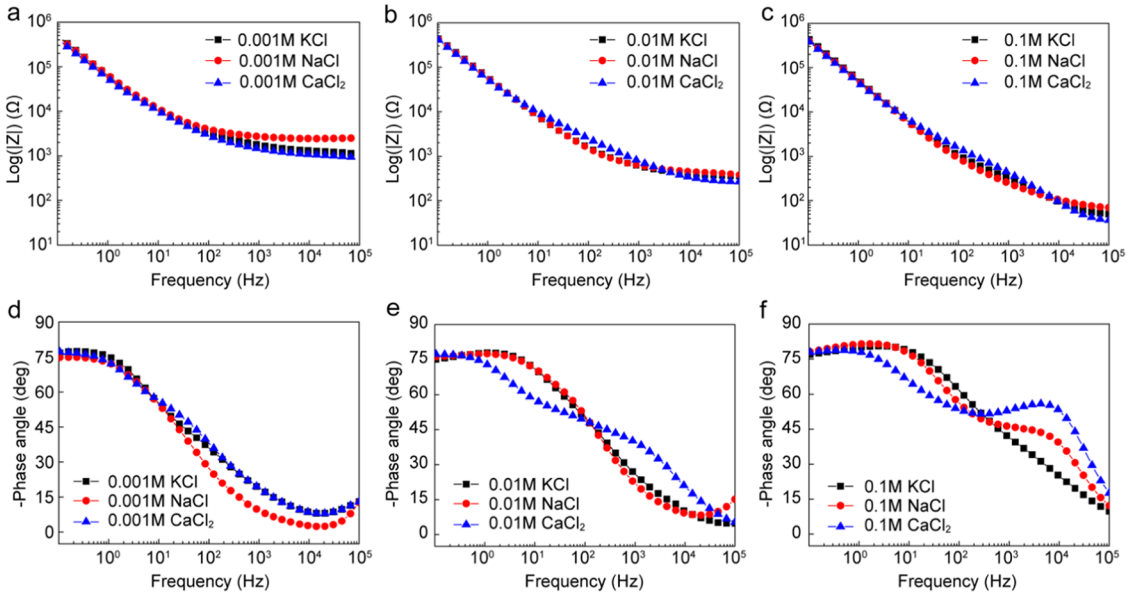

Figure 5. EIS results for 18CNTPs with a lipid bilayer according to cation and concentration: impedance of (a) 0.001 M, (b) 0.01 M, and (c) 0.1 M solution and phase angle of (d) 0.001 M, (e) 0.01 M, and (f) 0.1 M solution.

Electrochemical Analysis of SLBs and the Incorporation of CNTPs on the Au Electrode. CV tests were performed after the addition of lipids and CNTPs to analyze the variation in surface characteristics (see Figure S6). When compared to the bare electrode, the height of the redox curve of the lipid without AH was significantly reduced, indicating that the lipid was well covered on the electrode. Additionally, QCM-D analysis revealed that the covered lipid was a layer of vesicles (intact vesicle state). The signal strength was lower in lipids with AH, which acts as a trigger for the formation of the lipid bilayer, than in lipids without AH. Because the AH peptide is one of the most effective lipid bilayer-forming peptides, it can be used to demonstrate lipid bilayer formation.[32,34] The lipid bilayer incorporated with the CNTPs did not reach the current level of lipids with AH, but they did show effective surface covering. This suggests that the difference in current peaks with and without CNTPs is caused by ion transport through the CNTPs, i.e., the CNTPs in the lipid bilayer act as current paths between the electrode and solution. This configuration has much lower current values than the lipid electrode without AH, which is the vesicle layer, but higher than the lipid with AH. These findings indicate that the CNTPs effectively formed a lipid bilayer on the electrode surface.

EIS tests were conducted on the lipid bilayer with CNTPs of varying diameters on the Au electrode in the presence of a single cation (K^+, Na^+, and Ca^{2+}) at three different concentrations (0.001, 0.01, and 0.1 M). The Bode graphs in Figures 4 and 5 depict the cation transport effect of the 08CNTPs and 18CNTPs in the lipid bilayer. The range from

https://doi.org/10.1021/acs.jpcb.3c02917
J. Phys. Chem. B 2023, 127, 6316−6324

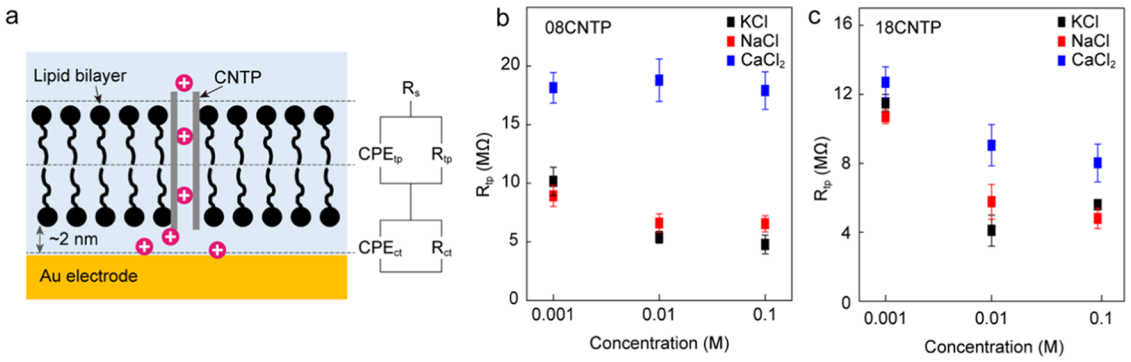

Figure 6. Schematic of equivalent circuit models and variation of membrane resistance (R_m). (a) Equivalent circuit model of SLBs on the Au. R_s is the solution resistance; CPE_{tp} is the capacitance generated owing to the ion transportation in the lipid bilayer; R_{tp} is the ion transport resistance of the lipid bilayer; CPE_{ct} is the capacitance on the Au electrode; and R_{ct} is the charge-transfer resistance on the Au electrode. Variation of membrane resistance (R_m) with ion concentrations as observed in the EIS tests: (b) 08CNTs in SLBs and (c) 18CNTs in SLBs.

10 Hz to 100 kHz in Bode plots indicated the formation of a lipid bilayer on the Au electrode.[37] As shown in the impedance plots (see Figures 4 and 5a−c), the highest impedance was detected in the lipid bilayer frequency range for all Ca^{2+} ion concentrations, regardless of the CNTP diameter. This indicated that Ca^{2+} ions increased the electrical resistance of the lipid bilayer by adsorbing onto its surface rather than being transported via the CNTP channel.[38] The impedance values of K^+ and Na^+ increased slightly with ion concentration, but the increase was less than that observed for the Ca^{2+} ions.

When the phase angle changes (see Figures 4 and 5d−f), the high-frequency spectra represent bilayer ionic transport resistance, whereas the low-frequency spectra represent interfacial charge transfer on the electrode.[39−41] The peaks of the phase angle in the high-frequency area increased with ion concentration in the Ca^{2+} ion solution, regardless of the CNTP diameter in the lipid bilayer. This is because Ca^{2+} ions bind with the lipid bilayer, and CNTP increases electrical resistance by reducing defects and blocking pores.[12,38] The K^+ and Na^+ ions showed similar properties; however, the increasing effect of the electrical resistance was weaker than Ca^{2+} ions. At low frequencies (below 10 Hz), as shown in Figure 4, the phase angle of Ca^{2+} for 08CNTPs incorporated in the lipid bilayer did not change significantly with ion concentration. Because Ca^{2+} ions are not able to be transported through the 08CNTP transmembrane channel, they have little effect on interfacial charge transfer on the Au electrode. Meanwhile, as the concentration of Ca^{2+} at 18CNTP incorporated in the lipid bilayer increased, the phase angle increased slightly due to the reduction of defects effect in the lipid bilayer, as shown in Figure 5. In contrast, K^+ ions significantly affected the Au electrode via CNTP in the lipid bilayer, as evidenced by a considerable increase in the phase angle with increasing ion concentration, regardless of the CNTP diameter. Na^+ ions showed a similar trend to K^+ ions, albeit to a lesser extent.

Similarly, ion transport resistance can be used to investigate differences in results based on ion type. The resistance values were calculated using the ZSimpWin software and an established equivalent circuit,[42−44] as shown in Figure 6a. Calculated results are shown in Tables S1 and S2. The circuit comprised serially connected impedance elements: the solution resistance (R_s), capacitance generated by the ion transport in the lipid bilayer (CPE_{tp}), the ion transport resistance of the lipid bilayer (R_{tp}), the capacitance of the Au electrode (CPE_{ct}), and charge-transfer resistance of the Au electrode (R_{ct}). Given the dispersion effect of solution resistance dispersion, microscopic electrode roughness, and difference in lipid bilayer morphology, a constant phase element (CPE) was used as a substitute for the ideal capacitance. Figure 6b,c shows the variations in the ion transport resistance of the lipid bilayer according to the K^+, Na^+, and Ca^{2+} ion concentrations, as obtained from the EIS tests.[45] Ca^{2+} ions showed the highest resistance for both types of CNTP diameters. For the 18CNTP incorporated in the lipid bilayer, for all types of ions, the R_{tp} values of the lipid bilayer gradually decreased as the ion concentration increased, owing to ion transport through the channel. Conversely, for the 08CNTPs incorporated in the lipid bilayer, changes in resistance were negligible during the test with Ca^{2+} ions because Ca^{2+} ions cannot pass through the channel. In the case of K^+ and Na^+, regardless of the CNTP diameter, the resistance decreased with increasing ion concentration. The phase angle variation at high and low frequencies strongly correlates with this result. The correlation between the resistance and phase angle variations of Ca^{2+} ions is related to the hydrated ion size. The diameter of the 18CNTPs is larger than the hydrated ion diameters (K^+: 0.66 nm, Na^+: 0.72 nm, and Ca^{2+}: 0.82 nm), allowing all ions to pass through the CNTPs.[46] It causes a decrease in ion transport resistance and an increase in phase angle at low frequencies. Ca^{2+} ions, on the other hand, could not be transported through 08CNTPs due to their size. Therefore, Ca^{2+} ions adsorbed onto the lipid bilayer and increased its rigidity with low defects rather than being transported to the electrode.[38] As the ion concentration was varied, this was observed as a small change in resistance and phase angle at high frequencies.

CONCLUSIONS

In this study, we have successfully demonstrated the formation of a rigid lipid bilayer incorporating CNTPs on Au electrodes using the AH peptides. The use of the FRAP test and QCM-D provided evidence for the formation of an SLB with embedded CNTPs. The EIS results revealed that regardless of the CNTP diameter, the R_{tp} of K^+ and Na^+ ions decreased with increasing ion concentration. The R_{tp} of the Ca^{2+} ion in 18CNTP is also affected by ion concentration, whereas negligible variation was observed for the 08CNTP channel owing to the hydrated ion size. The diameter of 18CNTPs is large enough for all ions to pass through, allowing the electrode to react with all ions. Ca^{2+}

https://doi.org/10.1021/acs.jpcb.3c02917
J. Phys. Chem. B 2023, 127, 6316−6324

ions, on the other hand, could not be transported through 08CNTPs due to their size. Therefore, Ca^{2+} ions adsorb onto the surface of the lipid bilayer rather than being transported to the Au electrode.

Our study demonstrates the potential use of the lipid bilayer on Au electrodes for ion sensors and selective transport, and our proof-of-concept platform could be extended with more complex architectures involving transmembrane proteins or surface-tuned artificial channels. Future research will focus on controlling the concentration of CNTP and other conductive substrates to further enhance the performance of this platform. Our findings pave the way for the potential for the development of new biosensing devices and biomimetic systems.

■ ASSOCIATED CONTENT

Supporting Information

The Supporting Information is available free of charge at https://pubs.acs.org/doi/10.1021/acs.jpcb.3c02917.

TEM image of CNTs; Cryo-TEM image of CNTs with vesicles; Raman spectra of the uncut CNTs; characterization of lipid bilayer formation on the Au electrode; CV tests; and summary of the calculated EIS test results (PDF)

■ AUTHOR INFORMATION

Corresponding Author

Kyunghoon Kim − *School of Mechanical Engineering, Sungkyunkwan University (SKKU), Suwon 16419, Republic of Korea;* orcid.org/0000-0001-8034-947X; Email: kenkim@skku.edu

Authors

Yunjeong Park − *School of Mechanical Engineering, Sungkyunkwan University (SKKU), Suwon 16419, Republic of Korea; Department of Electrical and Computer Engineering, Jack Baskin School of Engineering, University of California, Santa Cruz, Santa Cruz, California 95064, United States;* orcid.org/0000-0001-8541-6301

Minsung Hong − *Department of Advanced Materials Science and Engineering, Sungkyunkwan University (SKKU), Suwon 16419, Republic of Korea; Department of Nuclear Engineering, University of California at Berkeley, Berkeley, California 94720, United States*

Teayeop Kim − *School of Mechanical Engineering, Sungkyunkwan University (SKKU), Suwon 16419, Republic of Korea*

Hyeonseo Na − *School of Mechanical Engineering, Sungkyunkwan University (SKKU), Suwon 16419, Republic of Korea*

Sunho Park − *Department of Convergence Biosystems Engineering, Chonnam National University, Gwangju 61186, Republic of Korea; Department of Rural and Biosystems Engineering and Interdisciplinary Program in IT-Bio Convergence System, Chonnam National University, Gwangju 61186, Republic of Korea*

Yeon Ju Kim − *Department of Otolaryngology, Ajou University School of Medicine, Suwon 16499, Republic of Korea*

Jangho Kim − *Department of Convergence Biosystems Engineering, Chonnam National University, Gwangju 61186, Republic of Korea; Department of Rural and Biosystems Engineering and Interdisciplinary Program in IT-Bio Convergence System, Chonnam National University, Gwangju 61186, Republic of Korea;* orcid.org/0000-0001-9424-8215

Yun-Hoon Choung − *Department of Otolaryngology, Ajou University School of Medicine, Suwon 16499, Republic of Korea; Department of Medical Sciences, Ajou University Graduate School of Medicine, Suwon 16499, Republic of Korea*

Complete contact information is available at: https://pubs.acs.org/10.1021/acs.jpcb.3c02917

Author Contributions

[¶]Y.P. and M.H. contributed equally to this paper. They designed and performed the experiments. T.K. and H.N. fabricated and analyzed the CNTPs using Raman and UV−vis spectroscopy. Y.P., M.H., and H.N. performed the QCM-D measurements and electrochemical analyses. S.P. and Y.J. contributed additional insights and helped facilitate the progress of the study. Y.-H.C. and K.K. provided funding for the research. All authors have read and approved the final manuscript.

Notes

The authors declare no competing financial interest.

■ ACKNOWLEDGMENTS

This research was supported by the National Research Foundation of Korea (NRF) grants provided by the Korean Government (NRF-2023R1A2C2005617, NRF-2022M3A9H1014161, and NRF-2019M3A9H1103737). This work was also supported by a grant (NRF-2018H1A2A1062418) from the NRF, funded by the Korean Government (Global Ph.D. Fellowship Program).

■ REFERENCES

(1) Becucci, L.; Carbone, M. V.; Biagiotti, T.; D'Amico, M.; Olivotto, M.; Guidelli, R. Incorporation of the HERG potassium channel in a mercury supported lipid bilayer. *J. Phys. Chem. B* **2008**, *112*, 1315−1319.

(2) Krishna, G.; Schulte, J.; Cornell, B. A.; Pace, R. J.; Osman, P. D. Tethered Bilayer Membranes containing ionic reservoirs: selectivity and conductance. *Langmuir* **2003**, *19*, 2294−2305.

(3) Steinem, C.; Janshoff, A.; Ulrich, W.-P.; Sieber, M.; Galla, H.-J. Impedance analysis of supported lipid bilayer membranes: a scrutiny of different preparation techniques. *Biochim. Biophys. Acta* **1996**, *1279*, 169−180.

(4) Becucci, L.; Guidelli, R.; Peggion, C.; Toniolo, C.; Moncelli, M. R. Incorporation of channel-forming peptides in a Hg-supported lipid bilayer. *J. Electroanal. Chem.* **2005**, *576*, 121−128.

(5) Manzer, Z. A.; Ghosh, S.; Jacobs, M. L.; Krishnan, S.; Zipfel, W. R.; Piñeros, M.; Kamat, N. P.; Daniel, S. Cell-free synthesis of a transmembrane mechanosensitive channel protein into a hybrid-supported lipid bilayer. *ACS Appl. Bio Mater.* **2021**, *4*, 3101−3112.

(6) Mashaghi, S.; Jadidi, T.; Koenderink, G.; Mashaghi, A. Lipid nanotechnology. *Int. J. Mol. Sci.* **2013**, *14*, 4242−4282.

(7) Park, Y.; Kang, B.; Ahn, C. H.; Cho, H. K.; Kwon, H.; Park, S.; Kwon, J.; Choi, M.; Lee, C.; Kim, K. Bionanoelectronic platform with a lipid bilayer/CVD-grown MoS_2 hybrid. *Biosens. Bioelectron.* **2019**, *142*, No. 111512.

(8) Noy, A. Bionanoelectronics. *Adv. Mater.* **2011**, *23*, 807−820.

(9) Jackman, J. A.; Cho, N.-J. Model membrane platforms for biomedicine: case study on antiviral drug development. *Biointerphases* **2012**, *7*, 18.

(10) Sut, T. N.; Yoon, B. K.; Jeon, W. -Y.; Jackman, J. A.; Cho, N.-J. Supported lipid bilayer coatings: fabrication, bioconjugation, and diagnostic applications. *Appl. Mater. Today* **2021**, *25*, No. 101183.
(11) Tunuguntla, R. H.; Chen, X.; Belliveau, A.; Allen, F. I.; Noy, A. High-yield synthesis and optical properties of carbon nanotube porins. *J. Phys. Chem. C* **2017**, *121*, 3117−3125.
(12) Tunuguntla, R. H.; Escalada, A.; Frolov, V. A.; Noy, A. Synthesis, lipid membrane incorporation, and ion permeability testing of carbon nanotube porins. *Nat. Protoc.* **2016**, *11*, 2029−2047.
(13) Tunuguntla, R. H.; Henley, R. Y.; Yao, Y. C.; Pham, T. A.; Wanunu, M.; Noy, A. Enhanced water permeability and tunable ion selectivity in subnanometer carbon nanotube porins. *Science* **2017**, *357*, 792−796.
(14) Liu, L.; Xie, J. I.; Li, T.; Wu, H. C. Fabrication of nanopores with ultrashort single-walled carbon nanotubes inserted in a lipid bilayer. *Nat. Protoc.* **2015**, *10*, 1670−1678.
(15) Liu, L.; Yang, C.; Zhao, K.; Li, J.; Wu, H.-C. Ultrashort single-walled carbon nanotubes in a lipid bilayer as a new nanopore sensor. *Nat. Commun.* **2013**, *4*, No. 2989.
(16) Geng, J.; Kim, K.; Zhang, J.; Escalada, A.; Tunuguntla, R.; Comolli, L. R.; Allen, F. I.; Shnyrova, A. V.; Cho, K. R.; Munoz, D.; et al. Stochastic transport through carbon nanotubes in lipid bilayers and live cell membranes. *Nature* **2014**, *514*, 612.
(17) Chen, X.; Zhang, H. N.; Tunuguntla, R. H.; Noy, A. Silicon nanoribbon pH sensors protected by a barrier membrane with carbon nanotube porins. *Nano Lett.* **2019**, *19*, 629−634.
(18) Choi, M.-k.; Kim, H.; Lee, B. H.; Kim, T.; Rho, J.; Kim, M. K.; Kim, K. Understanding carbon nanotube channel formation in the lipid membrane. *Nanotechnology* **2018**, *29*, No. 115702.
(19) Hong, M.-S.; Park, Y.; Kim, T.; Kim, K.; Kim, J. -G. Polydopamine/carbon nanotube nanocomposite coating for corrosion resistance. *J. Materiomics* **2020**, *6*, 158−166.
(20) Hu, Z.; Wang, X.; Wang, W.; Zhang, Z.; Gao, H.; Mao, Y. Raman spectroscopy for detecting supported planar lipid bilayers composed of ganglioside-GM1/sphingomyelin/cholesterol in the presence of amyloid-*β*. *Phys. Chem. Chem. Phys.* **2015**, *17*, 22711−22720.
(21) Dresselhaus, M. S.; Dresselhaus, G.; Jorio, A.; Souza Filho, A. G.; Saito, R. Raman spectroscopy on isolated single wall carbon nanotubes. *Carbon* **2002**, *40*, 2043−2061.
(22) Bachilo, S. M.; Strano, M. S.; Kittrell, C.; Hauge, R. H.; Smalley, R. E.; Weisman, R. B. Structure-assigned optical spectra of single-walled carbon nanotubes. *Science* **2002**, *298*, 2361−2366.
(23) Spataru, C. D.; Ismail-Beigi, S.; Benedict, L. X.; Louie, S. G. Excitonic effects and optical spectra of single-walled carbon nanotubes. *AIP Conf. Proc.* **2005**, *772*, 1061.
(24) Chang, E.; Bussi, G.; Ruini, A.; Molinari, E. Excitons in carbon nanotubes: an ab initio symmetry-based approach. *Phys. Rev.* **2004**, *92*, No. 196401.
(25) Sun, X.; Zaric, S.; Daranciang, D.; Welsher, K.; Lu, Y.; Li, X.; Dai, H. Optical properties of ultrashort semiconducting single-walled carbon nanotube capsules down to sub-10 nm. *J. Am. Chem. Soc.* **2008**, *130*, 6551−6555.
(26) Keller, C. A.; Glasmästar, K.; Zhdanov, V. P.; Kasemo, B. Formation of supported membranes from vesicles. *Phys. Rev. Lett.* **2000**, *84*, 5443−5446.
(27) Keller, C. A.; Kasemo, B. Surface Specific kinetics of lipid vesicle adsorption measured with a quartz crystal microbalance. *Biophys. J.* **1998**, *75*, 1397−1402.
(28) Reviakine, I.; Brisson, A. Formation of supported phospholipid bilayers from unilamellar vesicles investigated by atomic force microscopy. *Langmuir* **2000**, *16*, 1806−1815.
(29) Bin, X.; Zawisza, I.; Goddard, J. D.; Lipkowski, J. Electrochemical and PM-IRRAS studies of the effect of the static electric field on the structure of the DMPC bilayer supported at a Au(111) electrode surface. *Langmuir* **2005**, *21*, 330−347.
(30) Zawisza, I.; Lachenwitzer, A.; Zamlynny, V.; Horswell, S. L.; Goddard, J. D.; Lipkowski, J. Electrochemical and photon polarization modulation infrared reflection absorption spectroscopy study of the electric field driven transformations of a phospholipid bilayer supported at a gold electrode surface. *Biophys. J.* **2003**, *85*, 4055−4075.
(31) Marquês, J.; De Almeida, R. F. M.; Viana, A. S. Lipid bilayers supported on bare and modified gold - formation, characterization and relevance of lipid rafts. *Electrochim. Acta* **2014**, *126*, 139−150.
(32) Cho, N.-J.; Frank, C. W.; Kasemo, B.; Höök, F. Quartz crystal microbalance with dissipation monitoring of supported lipid bilayers on various substrates. *Nat. Protoc.* **2010**, *5*, 1096−1106.
(33) Tabaei, S. R.; Choi, J.-H.; Zan, G. H.; Zhdanov, V. P.; Cho, N.-J. Solvent-assisted lipid bilayer formation on silicon dioxide and gold. *Langmuir* **2014**, *30*, 10363−10373.
(34) Cho, N.-J.; Cho, S.-J.; Cheong, K. H.; Glenn, J. S.; Frank, C. W. Employing an amphipathic viral peptide to create a lipid bilayer on Au and TiO_2. *J. Am. Chem. Soc.* **2007**, *129*, 10050−10051.
(35) Guo, H.; Xing, Q.; Huang, R.; Lee, D. W.; Su, R.; Qi, W.; He, Z. Real-time QCM-D monitoring of deposition of gold nanorods on a supported lipid bilayer as a model cell membrane. *ACS Omega* **2019**, *4*, 6059−6067.
(36) Ferhan, A. R.; Yoon, B. K.; Park, S.; Sut, T. N.; Chin, H.; Park, J. H.; Jackman, J. A.; Cho, N. -J. Solvent-assisted preparation of supported lipid bilayers. *Nat. Protoc.* **2019**, *14*, 2091−2118.
(37) Zhang, Y.; Inal, S.; Hsia, C.-Y.; Ferro, M.; Ferro, M.; Daniel, S.; Owens, R. M. Supported lipid bilayer assembly on PEDOT:PSS films and transistors. *Adv. Funct. Mater.* **2016**, *26*, 7304−7313.
(38) Melcrová, A.; Pokorna, S.; Pullanchery, S.; Kohagen, M.; Jurkiewicz, P.; Hof, M.; Jungwirth, P.; Cremer, P. S.; Cwiklik, L. The complex nature of calcium cation interactions with phospholipid bilayers. *Sci. Rep.* **2016**, *6*, No. 38035.
(39) Park, J.-S.; Choi, J.-H.; Woo, J.-J.; Moon, S.-H. An electrical impedance spectroscopic (EIS) study on transport characteristics of ion-exchange membrane systems. *J. Colloid Interface Sci.* **2006**, *300*, 655−662.
(40) Casero, E.; Parra-Alfambra, A.; Petit-Domínguez, M.; Pariente, F.; Lorenzo, E.; Alonso, C. Differentiation between graphene oxide and reduced graphene by electrochemical impedance spectroscopy (EIS). *Electrochem. Commun.* **2012**, *20*, 63−66.
(41) Bag, M.; Renna, L. A.; Adhikari, R. Y.; Karak, S.; Liu, F.; Lahti, P. M.; Russell, T. P.; Tuominen, M. T.; Venkataraman, D. Kinetics of ion transport in perovskite active layers and its implications for active layer stability. *J. Am. Chem. Soc.* **2015**, *137*, 13130−13137.
(42) Grossi, M.; Riccò, B. Electrical impedance spectroscopy (EIS) for biological analysis and food characterization: A review. *J. Sens. Sens. Syst.* **2017**, *6*, 303−325.
(43) Flynn, K. R.; Ackland, L.; Torriero, A. Electrochemical impedance spectroscopy study of the interaction of supported lipid bilayers with free docosahexaenoic acid. *Med. Anal. Chem. Int. J.* **2018**, *2*, No. 000122.
(44) Xiong, R.; Xiao, K.; Yi, P.; Hu, Y.; Dong, C.; Wu, J.; Li, X. The influence of Bacillus subtilis on tin-coated copper in an aqueous environment. *RSC Adv.* **2018**, *8*, 4671−4679.
(45) Diamanti, E.; Gutiérrez-Pineda, E.; Politakos, N.; Andreozzi, P.; Rodriguez-Presa, M. J.; Knoll, W.; Azzaroni, O.; Gervasi, C. A.; Moya, S. E. Gramicidin ion channels in a lipid bilayer supported on polyelectrolyte multilayer films: an electrochemical impedance study. *Soft Matter* **2017**, *13*, 8922−8929.
(46) Volkov, A.; Paula, S.; Deamer, D. Two mechanisms of permeation of small neutral molecules and hydrated ions across phospholipid bilayers. *Bioelectrochem. Bioenerg.* **1997**, *42*, 153−160.

https://doi.org/10.1021/acs.jpcb.3c02917
J. Phys. Chem. B 2023, 127, 6316−6324